Numerical Modeling of γ Precipitate Growth During Fe-Ni Martensite Decomposition at Low Temperatures ($\leq$400 °C)

J. ZHANG, D.B. WILLIAMS, and J.I. GOLDSTEIN

A numerical model was developed to simulate Ni composition profiles developed around γ (FeNi) precipitates growing during martensite (α_2) decomposition in Fe-Ni at low temperatures (300 °C to 400 °C). The model is based on the theory of partial interface reaction control of the precipitate growth process. Experimental Ni composition profiles were measured across γ-α_2 interfaces using high spatial resolution analytical electron microscopy. The simulated Ni composition profiles show good agreement with the experimentally measured profiles, indicating that partial interface reaction control of the γ growth is a reasonable assumption. The diffusion coefficients and the interface mobilities were estimated from the simulations. The activation energy for diffusion in the α_2 matrix obtained from the computer model is 0.7 eV with an error range from 0.58 to 0.98 eV. This value is similar to the activation energy for diffusion obtained from the calculated γ-α_2 interface mobility (0.62 eV with an error range from 0.57 to 0.67 eV). This result is consistent with the observed high dislocation density in the α_2 matrix. Both these values of the activation energy are well below that for lattice diffusion (~3 eV). Therefore, it is concluded that the prevailing diffusion mechanisms at these temperatures are short circuit (defect) diffusion in the α_2 matrix and rapid diffusion across the γ-α_2 interface.

I. INTRODUCTION

MARTENSITE (α_2) in Fe-Ni alloys is formed when the high-temperature face-centered cubic (fcc) γ phase is quenched to low temperatures. The α_2 decomposes when aged in the $\alpha + \gamma$ two-phase field of the Fe-Ni equilibrium phase diagram (Figure 1). During decomposition, fcc γ precipitates nucleate and grow in the α_2 matrix.[1] If the reaction were to proceed to equilibrium, the α_2 would transform into the body-centered cubic (bcc) α phase. In previous investigations,[1,2] α_2 decomposition has been used to determine the Fe-rich portion of the phase diagram above ~500 °C by direct measurement of the γ and α compositions. The compositions were measured using X-ray spectrometry in the electron probe microanalyzer (EPMA) or the analytical electron microscope (AEM). From these measurements, the $\gamma/\alpha + \gamma$ and $\alpha/\alpha + \gamma$ phase boundaries were determined.

At the low temperatures (<500 °C) used in this investigation, the situation becomes more complicated because the diffusivity of Ni in Fe is very low. Even after a 1 year heat treatment, the γ precipitates are very small (typically ~50-nm wide at 400 °C and ~10-nm wide at 300 °C). Accurate measurement of the precipitate composition therefore requires very high spatial resolution microanalysis. Furthermore, at low temperatures, the decomposition reaction does not go to completion and the γ precipitates form in a retained α_2 matrix. Depending on the rate-determining factor during γ precipitate growth, the Ni composition profile can assume different forms. If precipitate growth is diffusion controlled, *i.e.*, the chemical driving force required by the atoms to jump across the precipitate/matrix interface is minimal, then it is possible for the interface to reach equilibrium compositions. In this context, the term "diffusion control" means *any* diffusion mechanism that brings the solute atoms to the interface. However, it has been shown that for certain interface structures, it is difficult for atoms to diffuse across the interface at low temperatures.[4] Under these circumstances, the growth of the precipitate may be described in terms of "interface reaction control." Interface reaction control implies that the growth rate is determined by an interface reaction of some type, such as a ledge mechanism. In this case, the matrix composition can deviate significantly from equilibrium.[5] Thus, solute composition profiles across the precipitate/matrix interface will be different for the diffusion-controlled and the interface-reaction-controlled growth.

Detailed discussion of diffusion-controlled and interface-reaction-controlled growth can be found in many physical metallurgy textbooks (*e.g.*, References 5 and 6). In this article, we use the concept of "partial interface reaction control" (PIRC) to describe the situation where precipitate growth has a component of *both* diffusion and interface reaction control, but neither mechanism dominates. If PIRC growth occurs, the composition profile across the precipitate/matrix interface will be different from either diffusion control or interface reaction control. The differences in the solute composition profiles for different controlling mechanisms are illustrated schematically in Figure 2, and it is a basic tenet of this article, that accurate composition profile measurements can be used to distinguish between the three different control mechanisms.

From Figure 2, it is clear that to distinguish these growth mechanisms, the aging time should always be short enough so that the final equilibrium state is *not* reached since the final composition profiles are identical, regardless of the growth mechanism. As already

J. ZHANG, formerly Research Assistant, Department of Materials Science and Engineering, Lehigh University, is Staff Scientist, 3M Company, St. Paul, MN 55144. D.B. WILLIAMS, Professor, is with the Department of Materials Science and Engineering, Lehigh University, Bethlehem, PA 18015-3195. J.I. GOLDSTEIN, Professor, is with the Department of Mechanical Engineering, University of Massachusetts, Amherst, MA, 01003.

Manuscript submitted January 28, 1993.

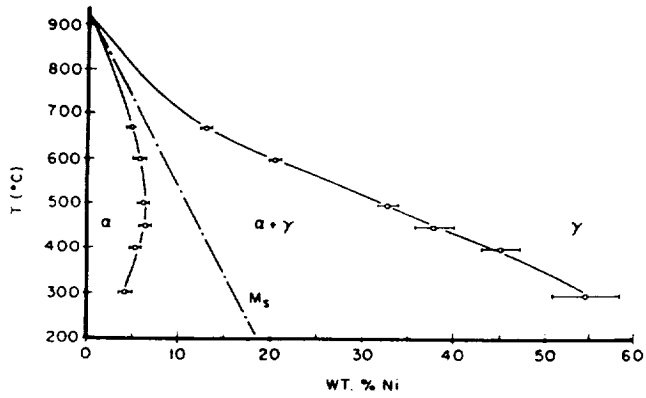

Fig. 1 — Fe-Ni binary phase diagram.[1,2,3]

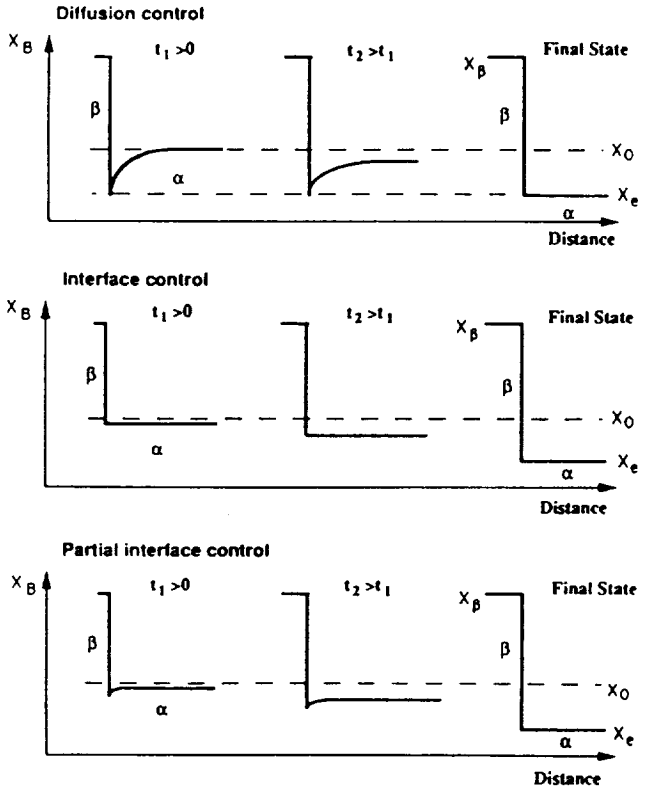

Fig. 2 — Schematic solute composition profiles at various stages of a precipitation process. The β-phase precipitates in α phase through different growth mechanisms. X_β, X_0, and X_e are the solute compositions of the precipitate phase, the alloy before precipitation, and the equilibrium matrix composition, respectively.

stated, this situation is easily achieved in the Fe-Ni system because of the slow Ni diffusion rates at temperatures $<\sim 500$ °C. Measuring the different composition profiles in Figure 2 requires accurate determination of the interfacial composition, which depends primarily on the spatial resolution of the analytical instrument. Current AEMs have a spatial resolution for elemental analysis of 2 to 10 nm, which is sufficient in certain cases to discern which of the three growth mechanisms in Figure 2 is operative.

In a recent experimental study on low-temperature Fe-Ni α_2 decomposition,[7] it was found that Ni composition profiles in the γ precipitates and the α_2 matrix, measured by X-ray energy dispersive spectrometry (EDS) in the AEM, did not agree with the tie-line equilibrium compositions given by the phase diagram. The γ-α_2 interface compositions measured in the decomposed α_2 were significantly higher than the values predicted by the phase diagram. More importantly, the width of the γ precipitates and the shape of the composition profiles in the α_2 could not be produced simultaneously by a diffusion-controlled growth model. In addition, the differences between the measured and the simulated composition profiles could not be attributed to errors in the compositional measurement. In order to account for these observations, the authors suggested that PIRC growth occurs.

In this article, a numerical model for the PIRC growth mechanism is presented. The interface mobility factor (M) is introduced, which independently determines the migration rate of the interface during an interface reaction. The overall precipitate growth is determined by a combination of M and the diffusion coefficient of Ni in α_2. Because α_2 contains a high density of defects (particularly dislocations), it is assumed that the diffusion coefficient used in the model reflects the more rapid, short-circuit diffusion characteristic of materials with a high defect density. This model is used to simulate precipitation during α_2 decomposition. The results of the simulation are in good agreement with the experimentally measured composition profiles using high spatial resolution AEMs. The values of M and the diffusion coefficients D are estimated by fitting the simulated profiles to the experimentally measured profiles. It is the purpose of this study to show that interface mobility, coupled with measured diffusion coefficients, can be used to model the composition profile across the γ-α_2 interface during low-temperature martensite decomposition in Fe-Ni alloys.

II. NUMERICAL MODEL

In this study, γ precipitate growth during α_2 decomposition was numerically simulated by diffusion control and PIRC models. One-dimensional planar growth is a reasonable assumption for both models, given that experimental profiles were only taken in regions where two planar γ precipitates were close to each other. In both models, diffusion occurs from the γ-α_2 interface to the midpoint in the α_2 matrix, where the diffusion zones of adjacent precipitates meet. This midpoint is referred to as the "impingement point," and the distance between the impingement point and the γ-α_2 interface is referred to as the "impingement distance." In both the diffusion and PIRC numerical models, volume diffusion in the matrix was simulated by solving Fick's second law using the Crank–Nicholson method[8] and the Murray–Landis variable grid technique.[9] The grid boundaries were set at the impingement point (the first point of the grid) and the γ-α_2 interface (nth point of the grid), as shown in Figure 3(a). The precipitate composition (X_p) is fixed. For both the diffusion and the PIRC models, the boundary condition at the impingement point is zero solute

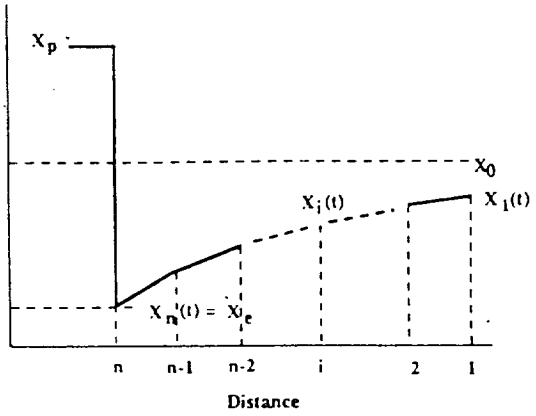

(*a*)

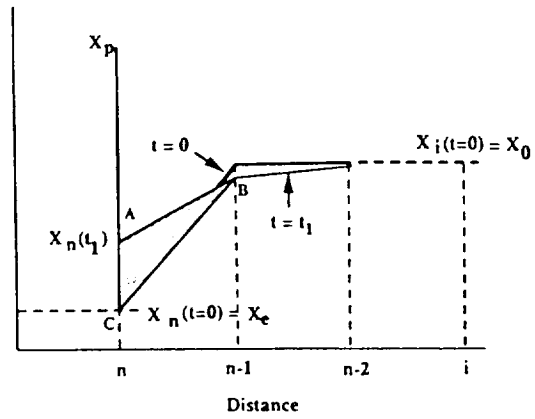

(*b*)

Fig. 3—(*a*) Schematic composition profile at an intermediate stage of precipitate growth according to the diffusion-controlled model superimposed on the grid scheme used in the numerical simulation. (*b*) Composition profiles at $t = 0$ and $t = \Delta t$ during precipitate growth according to the interface model. This diagram shows the method of adjusting the interface composition X_n as growth occurs.

flux; that is, the first-order derivative of the composition (X) with respect to distance (x) is zero (*i.e.*, $dX/dx = 0$).

A. *The Diffusion Model*

The major difference between the diffusion and PIRC models is the calculation of the γ-α_2 interface movement. The numerical solution to the diffusion model has been applied to the Fe-Ni system,[10] and the essentials of the model are briefly reviewed here. In the diffusion model, the boundary condition at the γ-α_2 interface is that the interface composition is a constant, *i.e.*, $X_n(t) = X_e$, as shown in Figure 3(a), where X_e is given by the phase diagram. For the given initial composition profile, at $t = 0$, the solute content in the α_2 matrix is $X_i = X_0$ ($i = 1, 2 \ldots n - 1$) and the interface composition is $X_n = X_e$.

The area (A) under the composition profile will decrease after each time increment by ΔA, as Ni solute atoms diffuse to the interface. The diffusion model assumes that all the Ni atoms that are brought to the interface can cross it. Therefore, the advance of the interface δ in each time increment Δt, *i.e.*, the growth of the precipitate, is calculated by

$$\delta = \Delta A/(X_p - X_e) \quad [1]$$

based on mass conservation. After each Δt, the position of the grid point n is changed due to the interface movement. The composition profile near the interface is slightly altered to keep X_n at X_e. The rest of the grid points (1 to $n - 1$) are rearranged using the Murray–Landis variable grid technique.[9] The error introduced into the simulation by the above process is negligible as long as Δt and δ are sufficiently small.

B. *Partial Interface Reaction Control Model*

In the PIRC model, the composition at the γ-α_2 interface is a constant for each time increment, Δt. However, the interface composition is adjusted between time increments according to mass conservation. In this case, the interface movement is independently calculated by

$$\delta = v\Delta t \quad [2]$$

$$v = M\Delta\mu/V_m \quad [3]$$

where v is the velocity of the interface, $\Delta\mu$ is the difference in chemical potential across the interface, M is the mobility of the interface, and V_m is the molar volume of the precipitate. An ideal solution is assumed for the simulation, so that

$$\Delta\mu = RT \ln (X_n/X_e) \quad [4]$$

In addition, the interface velocity can be expressed as

$$v = K \ln (X_n/X_e) \quad [5]$$

where

$$K = MRT/V_m \quad [6]$$

where R is the gas constant, T is the absolute temperature, X_n is the interface composition at any time, t, and X_e is the equilibrium interface composition. The term K has units of velocity. The interface velocity ($v(M,T)$) is determined by the ability of the Ni atoms to jump across the interface. For a certain set of variables (T, D, M, X_n ...) within a time increment, Δt, the number of atoms brought to the interface, ΔA, might be greater than, equal to, or less than the number of atoms able to jump across the interface, $\delta(X_p - X_n)$. If $\Delta A < \delta(X_p - X_n)$ at any time, the growth is diffusion-controlled by definition. The PIRC model only deals with the situation where $\Delta A \geq \delta(X_p - X_n)$ at the beginning of the γ growth process.

The numerical solution to the PIRC model assumes that when $t = 0$, $X_n = X_e$. Therefore, there is no interface movement ($v = 0$) after the first time increment ($t = 1$) according to Eqs. [3] and [4]. To ensure mass conservation during this first time increment, the change of area under the composition profile ΔA (equal to the area of triangle ABC in Figure 3(b)) is added to the composition profile near the interface region. This addition of mass has the effect of increasing the interface composition $X_n(t = 0)$ to $X_n(t_1)$ and altering the composition profile between the interface and the next sampling

point, X_{n-1} (Figure 3(b)). The decrease of Ni solute content from the original composition profile X_{n-1} ($t = 0$) to X_{n-1} (t_1) (point B in Figure 3(b)) is due to diffusion. In this calculation, it is assumed that the interface has an effective thickness of one grid spacing. This is a reasonable assumption since one grid spacing corresponds to ≤ 1 nm in the actual simulations. The adjustment of X_n in the model, required by conservation of mass, is equivalent to a situation where the Ni atoms pile up at the interface, thus raising the chemical potential difference across the interface. (After the first step, X_n could either increase further or decrease, depending on whether Ni diffusion to the interface or the interface reaction is faster. On average, taken over many time increments, it is expected that X_n will decrease slowly with time as the matrix Ni content at the impingement point decreases.) In the next time increment ($t = t_2$), the composition in the α_2 will be calculated using $X_n(t_1)$ as the boundary condition at the γ-α_2 interface. Since X_n is no longer equal to X_e, $\Delta\mu$ is no longer zero and the velocity of the interface can be calculated (Eq. [3]). In this process, it is necessary to assume a first iteration value for D and M (actually K in Eq. [6]). As shown later in Figure 5, it is possible to predict the manner in which the composition profile changes for specific changes in D and M, so reasonable values are chosen based on the diffusion coefficients of Romig and Goldstein[11] and the measured interface velocities. If unreasonable values are chosen, then the model cannot predict reasonable composition profiles that are consistent with several known and measurable variables such as the γ-α_2 interface composition, the composition of the impingement point, and the width of the γ precipitate.

During the first few time increments, it is possible that insufficient Ni atoms will diffuse to the interface such that $\Delta A < \delta(X_p - X_n)$. While this situation technically violates the PIRC conditions, it will be corrected in the next time increment. The simulation program can handle the situation where $\Delta A < \delta(X_p - X_n)$ as long as it does not require that $X_n < X_e$. After a few initial oscillations in ΔA, a dynamic balance will be established between the advancing interface reaction front and diffusion in the α_2 matrix so that, at any time, the number of Ni atoms which diffuse to the interface is approximately equal to the number of Ni atoms that cross it during the interface reaction. The interface composition X_n, after a transient fluctuation at the beginning, is stabilized at a certain value *greater* than X_e. As just noted, the value of X_n is much higher than X_e and will decrease as γ growth proceeds. This decrease in X_n occurs because ΔA decreases as the Ni concentration at the impingement point ($X_m(t)$) decreases. Eventually, $\Delta A < \delta(X_p - X_n)$ and γ growth effectively ceases. The value of X_n and, therefore, the composition gradient in the matrix varies with time and is determined by the values of D and M.

The preceding scenario will only occur for certain combinations of M and D (the diffusion coefficient of Ni in the matrix). If the value of M is very small, a large $\Delta\mu$ is needed for γ growth such that $X_n \approx X_0$ (Figure 2). In this case, growth is completely interface-reaction controlled. If the value of M is large, then $X_n = X_e$, and the growth will be diffusion-controlled. The PIRC mechanism will operate between these two extremes.

The scheme used for adjusting the γ-α_2 interface composition to calculate the solute composition at the interface is valid only if conservation of mass is obeyed. The total area underneath the precipitate and the α_2 matrix composition profiles (*i.e.*, the total mass) was monitored from time to time in the simulation. The ratio between the total areas before and after γ growth was always very close to one (to the fourth decimal place) and did not increase with time for all values of T and D used in this study.

III. SIMULATIONS

The bulk Ni composition, X_0, and the total diffusion time (equal to the aging time of the alloys)[7] were used in the simulations. The impingement distances measured in the alloys were used in the simulations after being adjusted so that the γ-α_2 volume ratio was that present in three-dimensional space (even though the diffusion equation is solved in one-dimensional space). The compositions of the $\alpha/\alpha + \gamma$ boundary in the Fe-Ni phase diagram[12] were used for X_e, and the Ni contents of the γ precipitates measured in the alloys[7] were used for X_p. The diffusion coefficients (D), and the interface mobility factor (M) for the interface-reaction-controlled model, were systematically varied to achieve the best fit between the simulated and the experimentally measured Ni composition profiles. The Ni diffusion coefficients (D) in dislocation-rich α_2 measured below 410 °C by Romig and Goldstein[11] were used as starting values. The activation energy is 0.46 ± 0.15 eV and D_0 is (3.6 ± 3) × 10^{-15} cm^2/s. The choice of this particular diffusion coefficient is considered reasonable because of the high dislocation density observed in the α_2 matrix. The microstructures of the α_2 in this study and that in the Romig and Goldstein[11] study are essentially identical.

Figure 4 shows simulated Ni composition profiles for γ precipitate growth. Two different times were assumed for the diffusion and the PIRC models. For the diffusion model, both the α_2 matrix composition and the composition gradient vary with time. However, for the PIRC model, only the composition of the α_2 matrix varies with time and the composition gradient remains almost constant with time. It should be noted that the diffusion model produces a similar sized precipitate as the PIRC model for the same diffusion coefficient and one-fifth the time. In Figure 4, a slow interface reaction rate or small interface mobility (M) was used. A high interface composition (X_n) was obtained, which decreased the composition gradient available in the matrix.

Figure 5 shows simulated composition profiles for the PIRC model under different combinations of D and M (or the velocity coefficient, K, from Eq. [6]). If K is sufficiently large, as in Figure 5(a), the profile is similar to that generated by the diffusion model. Decreasing K will increase the interface composition and change the slope of the composition profile in the α_2 matrix (Figure 5(b)). Increasing D has the same effect on the slope of the composition profile (Figure 5(c)). If D is relatively large and K is sufficiently small (Figure 5(d)), the composition profile in the α_2 matrix is almost flat. It is clear from these simulations that for PIRC growth,

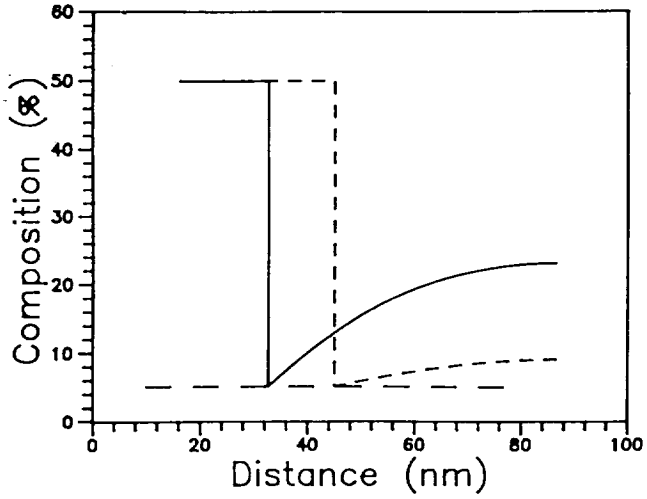

(*a*)

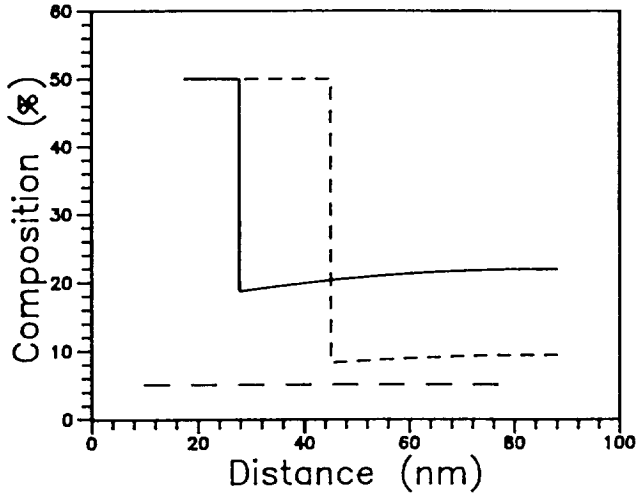

(*b*)

Fig. 4—Comparison of the simulated Ni composition profiles using the diffusion and PIRC growth models with $X_r = 0.05$, $X_p = 0.50$, $X_0 = 0.25$, $T = 673$ K, and a 70 nm impingement distance. (*a*) The diffusion model, $D = 3 \times 10^{-18}$ cm^2/s; solid line $t = 480$ h, dashed line $t = 1800$ h. (*b*) the PIRC model, $D = 3 \times 10^{-18}$ cm^2/s and $K = 8 \times 10^{-7}$ nm/s; solid line $t = 2400$ h, dash line $t = 8880$ h.

a large diffusion coefficient does not necessarily yield a bigger γ precipitate (compare Figures 5(a) and 5(d)) . What is important is the coupling of D and K.

IV. EXPERIMENTAL

Fe-Ni alloys used in this study were made from high-purity (99.998 pct) Fe and Ni rods. The alloys were melted in a vacuum induction furnace and homogenized in the single-phase γ field at 1200 °C for 7 days. To prevent oxidation, each alloy was sealed in a quartz tube that was evacuated and refilled with argon. A piece of tantalum foil was placed in the tube as an Oxygen absorber. After homogenization, the alloys were quenched first in water and then in liquid nitrogen in order to form α_2. The homogeneity of each alloy was analyzed using X-ray wavelength dispersive spectrometry (WDS) in a JEOL 733 EPMA. The homogeneity range and homogeneity level were calculated using the equations given by Goldstein *et al.*[12] For each alloy, the composition, homogeneity level, and microstructure, as observed in the optical microscope and the scanning electron microscope (SEM), are listed in Table I. Thin foils for AEM study were prepared by first cutting each homogeneous alloy into 3-mm-diameter rods using an electric discharge machine. These rods were separately sealed in quartz tubes as just described for bulk alloy homogenization. Isothermal heat treatments were conducted in horizontal furnaces with an LFE model 2000 microprocessor temperature controller. The error in the heat treatment temperatures, determined by the accuracy of the thermocouple and the controller, was less than ±4 °C over time periods of up to 1 year. The alloys were quenched in water after heat treatment. The heat treatment time and temperature of each alloy specimen are also listed in Table I. The first three digit number in each alloy label indicates the heat treatment temperature in degrees Celsius. The two digit number following the FN (Fe-Ni) designation indicates the nominal Ni composition of the alloy.

Two AEMs were used to measure the α_2 and γ compositions: a 300 keV PHILIPS* EM430T equipped with a Link intrinsic Ge EDS detector and a 100 keV Vacuum Generators (VG) HB501 equipped with a Link Si(Li) EDS detector. Both EDS detectors were controlled by a Link AN10000 MCA/computer system. The electron source was a LaB_6 filament for the PHILIPS and a cold field emission gun (FEG) for the VG. The electron probes were systematically characterized in order to calculate the spatial resolution of the X-ray analysis. The electron optical conditions used for the X-ray analysis were a 50-μm C2 aperture and a 7-nm-diameter full-width at half-maximum (FWHM) probe for the EM430T, and a 50-μm virtual objective aperture and a 1-nm-diameter (FWHM) probe were used for the HB501. These were the optimum conditions under which the electron probe had a near-Gaussian intensity distribution and yielded spatial resolutions approaching the theoretically calculated values.[13,14]

*PHILIPS is a trademark of Philips Electronic Instruments, Corp., Mahwah, NJ.

The Cliff–Lorimer ratio equation[15] was used to calculate the Fe and Ni compositions (C_{Fe}, C_{Ni}) from the characteristic X-ray intensities above background (I_{Fe}, I_{Ni}):

$$C_{Fe}/C_{Ni} = k_{FeNi}(I_{Fe}/I_{Ni}) \quad [7]$$

The k_{FeNi} sensitivity factors were experimentally measured for each microscope.[16] X-ray absorption in the Fe-Ni system was negligible (<±2 pct) for the instrumental and specimen conditions used in this study.

The specimen thickness was measured using the X-ray count method.[14] A calibration curve of X-ray counts/pA/min (over the energy range 0 to 10 keV) from an Fe-25 wt pct Ni specimen was plotted as a function of specimen thickness for each AEM. Typical specimen thicknesses where the EDS analysis was performed were

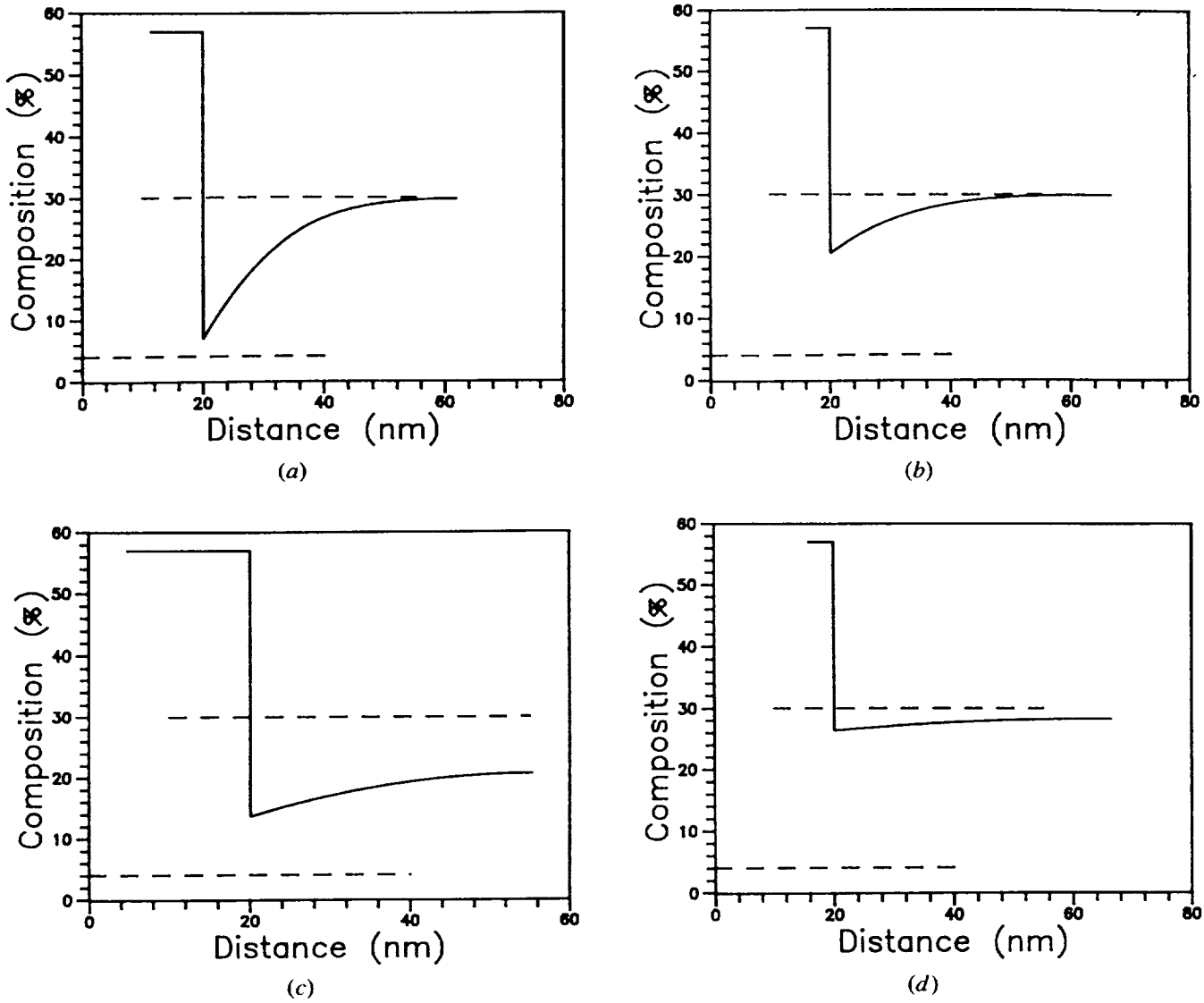

Fig. 5—Composition profiles simulated by the PIRC model showing the effect of D and K on the interface composition, precipitate width, and the composition gradient in the matrix. The parameters of the simulations were $X_\gamma = 0.04$, $X_\beta = 0.57$, $X_0 = 0.30$, $t = 8880$ hours, $T = 573$ K, and 50 nm impingement distance. (*a*) $D = 5 \times 10^{-20}$ cm^2/s, $K = 3 \times 10^{-7}$ nm/s. (*b*) $D = 5 \times 10^{-20}$ cm^2/s, $K = 6 \times 10^{-8}$ nm/s. (*c*) $D = 4 \times 10^{-19}$ cm^2/s, $K = 3 \times 10^{-7}$ nm/s. (*d*) $D = 4 \times 10^{-19}$ cm^2/s, $K = 6 \times 10^{-8}$ nm/s.

40 to 100 nm for the PHILIPS AEM and 10 to 20 nm for the VG. The specimen drift was corrected by software in the Link AN10000 which periodically checks an operator-specified feature in the analyzed area for any specimen drift and moves the electron probe accordingly. The spatial resolution of the X-ray analysis was calculated using the equations of Reed[117] and Michael *et al.*[118] In all cases, the spatial resolution was estimated assuming that there was a discrete composition change at the α_2-γ interface and the interface was aligned parallel to the electron beam. If the interface was not well aligned, then the apparent spatial resolution would always be greater than the best expected value.

V. AEM RESULTS

Figure 6 shows a Ni composition profile across the interface between the γ (high Ni content precipitate) and the low Ni α_2 matrix in the 400FN30 alloy. This profile was measured using the EM430T AEM and has an estimated spatial resolution of ~12 nm. The simulated composition profiles for both the diffusion model (dashed line) and the PIRC model (solid line) are also plotted in Figure 6. For the diffusion model, D was chosen so that the half-width of the precipitate in the simulated profile was the same as that measured experimentally. If the diffusion model applied, the AEM should be able to measure the composition profile accurately. If D was chosen so that a very narrow Ni depletion zone was present near the interface (*i.e.*, below the spatial resolution of the AEM), then the width of the γ precipitate would be much less than the smallest precipitate observed in the alloy. Therefore, the diffusion model cannot fit the experimentally measured data. A unique combination of D and K was found such that the PIRC model fit both the half-width of the γ precipitate

Table I. Heat Treatment Time and Temperature for the Experimental Alloys

Alloy	400FN30	400FN25	350FN30	300FN30
Ni (wt pct)	29.6	25.0	29.6	29.6
Homogeneity level (pct) at 99 pct confidence level	0.5	0.3	0.5	0.5
Microstructure before aging	plate martensite	lath martensite	plate martensite	plate martensite
Heat treatment temperature (°C)	400	400	350	300
Time (days)	362	362	400	370

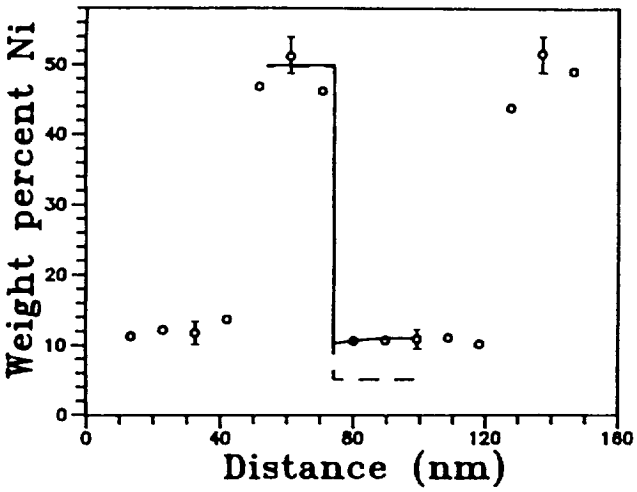

Fig. 6—Experimentally measured Ni composition profile in the 400FN30 alloy and the simulated composition profiles using the diffusion model (dashed line), $D = 10^{-17}$ cm^2/s, and the PIRC model (solid line), $D = 1.7 \times 10^{-18}$ cm^2/s and $K = 4.6 \times 10^{-7}$ nm/s.

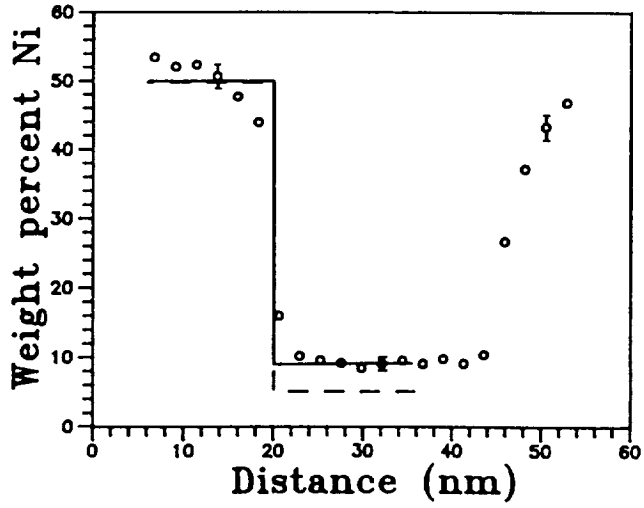

Fig. 7—Experimentally measured Ni composition profile in the 400FN25 alloy and the simulated composition profiles using the diffusion model (dashed line), $D = 10^{-17}$ cm^2/s, and the PIRC model (solid line), $D = 7.3 \times 10^{-19}$ cm^2/s and $K = 2.8 \times 10^{-7}$ nm/s.

and the slope of the composition profile in the α_2 matrix at the same time.

A Ni composition profile across an α_2-γ interface in the 400FN25 alloy measured using the VG is shown in Figure 7. The estimated spatial resolution for this measurement is ~3 nm. Unfortunately, the actual spatial resolution seems to be >3 nm, probably because the interface was not perfectly parallel to the electron beam. Again, the composition profile generated from the diffusion model does not fit the experimental data, either near the interface or in the middle of the matrix. However, the PIRC model with a unique combination of D and K does fit the data quite well.

Figure 8 shows a Ni composition profile across an α_2-γ interface in the 300FN30 alloy, measured using the VG. At 300 °C, the precipitate is rather small and the α_2 Ni composition is significantly higher than the equilibrium value. The measured compositions have relatively larger errors (~±10 pct relative) than those measured in the high-temperature alloys (~±5 pct relative). Nevertheless, only the PIRC model gives a reasonable fit, both to the half-width of the γ precipitate and to the slope of the α_2 matrix composition profile simultaneously. The diffusion model yields a depletion zone (dashed line in Figure 8), which should have been detectable in the VG AEM (spatial resolution ~2 nm) if it was present, even considering any slight misalignment of the interface with respect to the electron beam.

Table II lists the numerical values of D and K for the

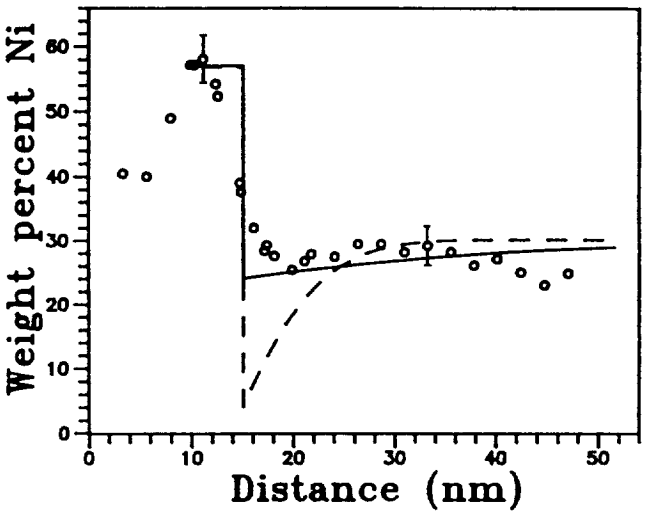

Fig. 8—Experimentally measured Ni composition profile in the 300FN30 alloy and the simulated composition profiles using the diffusion model (dashed line), $D = 10^{-17}$ cm^2/s, and the PIRC model (solid line), $D = 1.9 \times 10^{-19}$ cm^2/s and $K = 7.3 \times 10^{-8}$ nm/s.

four alloys (Table I) obtained by fitting the simulated composition profiles to the experimentally measured profiles. The interface mobility, M, calculated for each alloy according to Eq. [6] with $V_m = 7 \times 10^{-6}$ m^3/mol, is also included in Table II. The physical meaning and

Table II. Calculated Diffusion Coefficients and Interface Mobility Factors

Alloy	T	D (cm^2/s)	K (nm/s)	M (m^2 s/kg)
400FN30	673	$1.7(1.3 \text{ to } 2.3) \times 10^{-18}$	$4.6(4.1 \text{ to } 5.0) \times 10^{-7}$	5.8×10^{-25}
400FN25	673	$4.0(2.5 \text{ to } 4.5) \times 10^{-18}$	$3.8(3.5 \text{ to } 4.1) \times 10^{-7}$	4.8×10^{-25}
350FN30	623	$7.3(6.5 \text{ to } 7.6) \times 10^{-19}$	$2.8(2.6 \text{ to } 3.1) \times 10^{-7}$	3.8×10^{-25}
300FN30	573	$1.9(1.2 \text{ to } 2.3) \times 10^{-19}$	$7.3(6.9 \text{ to } 8.1) \times 10^{-8}$	1.1×10^{-25}

the error for each parameter in Table II will be discussed in Section VI.

VI. DISCUSSION

A. *Errors in the Diffusion Coefficients and the Interface Mobilities*

The first source of error for the diffusion coefficients and the interface mobilities obtained in this study is due to the error in the composition measurements. The statistical error in the X-ray EDS analysis, given by twice the standard deviation of the peak X-ray counts collected, or at 95 pct confidence level, was typically ±5 to 10 pct relative for the matrix phase. Due to the limited number of data points in each composition profile, no strict mathematical fitting procedure was used in this study to fit the experimental composition profiles with the simulated ones. Instead, three parameters were used to determine a good fit: (1) the width of the γ precipitate; (2) the α_2 matrix phase composition at the γ-α_2 interface; and (3) the α_2 matrix phase composition at the impingement point. This method is valid since the composition profiles in the α_2 are smooth. Also, the profile slopes are governed by the diffusion process and the boundary conditions at both the interface and the impingement point. A ± 10 pct relative error, which translates into a ±1 wt pct and a ±3 wt pct error in the measured compositions for a 10 wt pct and a 30 wt pct α_2 composition, respectively, will result in a variation in D and K of a factor of ~1.5. Therefore, the D and K factors determined are accurate to approximately ±50 pct relative if only statistical errors are considered.

Other sources of error are the limited spatial resolution of the AEMs used in the composition measurements and the nonoptimum geometry condition of the precipitate being analyzed. Both of these factors result in a measured composition profile that deviates from the true composition profile. The error introduced from these two sources is not random but always overestimates the interface composition. Therefore, the D value is overestimated and the K value underestimated. (Figure 5 shows the effect of D and K on the shape of composition profile.) Among the three parameters used for the fitting, only the interface composition could potentially be affected seriously because the composition variation with distance from the impingement point is usually very small and the precipitates are usually 3 to 5 times wider than the spatial resolution of the AEMs being used. For the composition profiles measured in the high-temperature alloys, the composition gradients are rather small and the error of the measured interface composition is negligible compared to the statistical uncertainty. However, for the low-temperature alloy, where a relatively large composition gradient exists near the interface, the error of the measured interface composition must be taken into account. During the simulation, this error was compensated for by fitting the simulated composition profile with a lower interface composition (Figure 8, interface model) determined from the extrapolation of the measured α_2 matrix composition to the interface, instead of fitting with the measured interface composition directly.

Finally, an error in the measurement of D and K could be a result of the alloy system itself. It has been shown in this study that the dominant diffusion mechanism in low-temperature Fe-Ni martensite decomposition is short-circuit diffusion and the growth is partially controlled by the interface reaction. (This point is discussed in more detail in Section 2.) Therefore, both the D and K values are strongly dependent on the defect structure. Since the local defect structure and the γ-α_2 interface structure (ledge structure, for example) could vary, the D and K coefficients could vary from place to place in the same alloy. Transmission electron microstructural observations show that there is a γ precipitate size distribution in each alloy. This distribution possibly reflects the difference in D and K due to local (defect) structure variations. It is possible that the large diffusion coefficients determined previously for the Fe-Ni martensite at 300 °C[11] are due to this same effect, because at that time, it was necessary to choose the largest precipitate in the alloy so that an AEM analysis could be obtained. In this study, special care was taken to choose the most typical γ precipitates in terms of their sizes and local structures. However, this selection method used was still subjective and by no means statistically rigorous.

Using the errors in D and K, the error in the activation energy was determined using the marginal D and K values. These errors are shown in Figures 9 and 10. The calculated activation energies have nonsymmetrical error bars.

B. *Diffusion Coefficient and Interface Mobility*

The natural logarithm of the diffusion coefficients of the 30 wt pct Ni alloys (Table II) are plotted against $1/T$ in Figure 9. The calculated activation energy, ΔE, obtained from the data in Figure 9 is 0.7 eV, with an error range from 0.58 to 0.98 eV, and D_0 is 5.5×10^{-13} cm^2/s. As already stated, previous studies of diffusion in α_2 at temperatures <410 °C[11] reported an activation energy of 0.46 ± 0.15 eV.

The interface mobility factor (M) between a growing phase (or grain) and a shrinking phase (or grain) is given by

$$M = (A_c n \nu V_m^2)/N_a RT \exp(-\Delta G_a/RT) \quad [8]$$

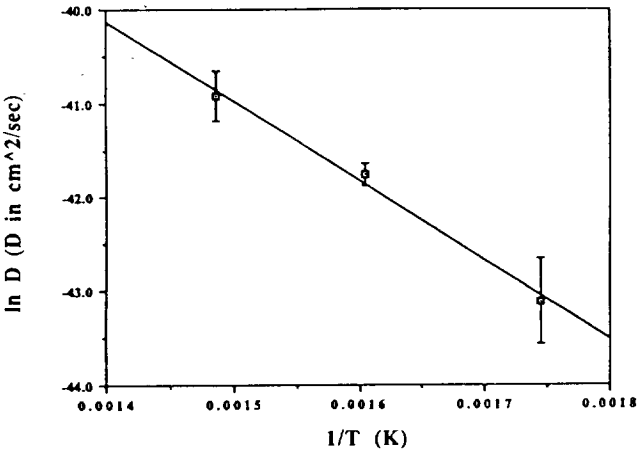

Fig. 9—ln D *vs* $1/T$ plot for the 30 wt pct Ni alloys.

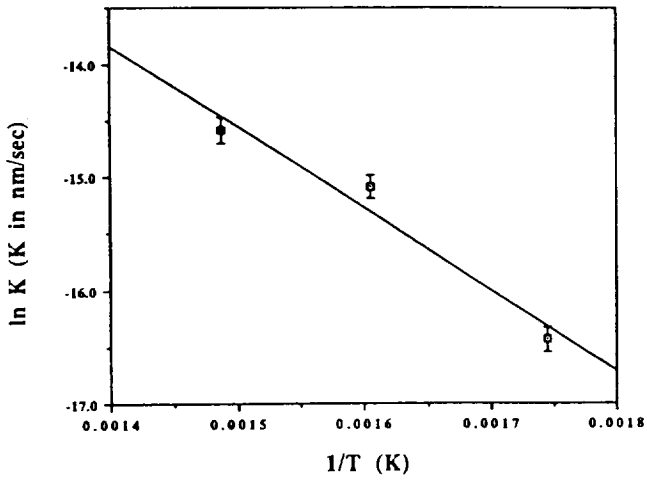

Fig. 10—ln K *vs* $1/T$ plot for the 30 wt pct Ni alloys.

where A_c is the accommodation factor of the interface (the probability that the jumping atom will remain in the same atomic site). The pertinent value of A_c is on the side of the interface, which is growing (*i.e.*, the γ precipitate side in the case of precipitate growth), n is the number of atoms per unit area, which are in energetically favorable sites to jump across the interface on the side of the interface that is shrinking (*i.e.*, the α_2 matrix side in this case), ν is the vibration frequency of the atoms, ΔG_a is the molar activation energy for lattice diffusion (which equals $N_a \Delta E$, where N_a is Avogadro's number).[6] The temperature dependence of M with time is not exponential (Eq. [8]). However, the interface velocity factor (K) has an exponential dependence on temperature according to Eq. [6]. Combining Eq. [6] and [8] we obtain

$$K = (A_c n \nu V_m)/N_a \exp(-\Delta G_a/RT) \qquad [9]$$

A ln K *vs* $1/T$ plot for the 30 wt pct Ni alloys is shown in Figure 10. The calculated activation energy for diffusion obtained from the interface mobility is 0.62 eV with an error range from 0.55 to 0.67 eV, which is almost equivalent to the activation energy for diffusion obtained from the computer simulation of the Ni composition profiles (0.7 eV). This similarity is reasonable because the energy barrier to diffusion between adjacent lattice sites is lowered at an interface between two different crystal structures and is also lowered in a lattice containing a high density of line defects. In both cases, the activation energy should be lower than typical activation energies for diffusion in a perfect lattice (~3 eV).

As just stated, the value of the activation energy calculated in this study for Ni diffusion in the α_2 and the value determined from the interface mobility (M) during the interface reaction are very close. This similarity suggests that the diffusion mechanism for the γ growth at low temperatures is *not* bulk volume diffusion, which involves vacancy generation and has a much higher activation energy (~3 eV). That the proposed mechanism is defect diffusion is not surprising from the structural point of view, since it might be expected that diffusion is controlled by defects in the α_2, as discussed by Romig and Goldstein.[11] Structural observations in these alloys[7] confirmed that the γ precipitates were formed in an α_2 matrix that contained a high dislocation density. The activation energies from previous diffusion analyses can be compared with the results obtained in this study. Previous studies of α_2[11] reported an activation energy of 0.46 ± 0.15 eV for diffusion at temperatures <410 °C. In contrast, high-temperature (500 °C to 900 °C) studies of diffusion in bcc, dislocation-poor ferrite (α)[19,20] reported an activation energy of ~3.03 eV. Clearly, the activation energy for diffusion measured in this study (0.7 eV) is much closer to that for low temperature (<410 °C) Fe-Ni martensite (0.46 ± 0.15 eV). The best-fit D_0 value determined in this study is 5.5×10^{-13} cm^2/s and is much higher than the D_0 of $(3.6 \pm 3) \times 10^{-15}$ cm^2/s of Romig and Goldstein.[11] Differences in the activation energy and the D_0 values between this study and that of Romig and Goldstein appear to be significant. However, comparison of actual diffusivity (D) values at 400 °C, (1.7 to 4) $\times 10^{-18}$ cm^2/s in this study *vs* (0.6 to 1) $\times 10^{-18}$ cm^2/s by Romig and Goldstein, and at 300 °C, (1.2 to 2.3) $\times 10^{-19}$ cm^2/s in this study *vs* (1 to 3) $\times 10^{-19}$ cm^2/s by Romig and Goldstein, show that the calculated D values in this study are very close. The agreement in the values of the diffusion coefficient measurement in the two studies again argues that the high dislocation density in the α_2 microstructure controls the diffusion process.

The intercept of the ln K *vs* $1/T$ plot (Figure 9) at $1/T = 0$ is 2.24×10^{-11} m/s. This intercept permits determination of a value of the accommodation factor, A_c, since

$$K_0 = (A_c n \nu V_m)/N_a \qquad [10]$$

If we use a common value of $\nu \sim 10^{-13}$ and $n = 1.7 \times 10^{19}$/m^2 for the {110} plane of a bcc structure with $a_0 = 0.287$ nm, then A_c is $\sim 10^{-14}$. It should be noted that for a given K_0, A_c is inversely proportional to n, which is the number of atoms in energetically favorable positions per unit area. If the α/γ interface were faceted, as expected for a semicoherent interface, the estimated A_c could be much larger because n would be much smaller. Another factor that should be considered is that the growth may be by a ledge mechanism.[21,22]

VII. SUMMARY

1. A numerical model was developed to account for the effect of the interface reaction on the γ precipitate growth process. This model also incorporates diffusion and is thus termed the PIRC model.
2. The PIRC numerical model was applied to γ precipitate growth during the decomposition of α_2 (Fe-Ni martensite) at low temperatures ($\leq$400 °C). The composition profiles measured by high spatial resolution (2 to 10 nm) AEM were successfully simulated by the numerical model. Therefore, we conclude that γ growth in the low-temperature Fe-Ni α_2 decomposition is under partial interface reaction control.
3. The diffusion coefficients (D) of the α_2 and the velocity coefficients (K) of the semicoherent interface between the high Ni γ fcc precipitate and the α_2 matrix were determined. The activation energies of the atomic migration in the α_2 matrix and the interface were calculated from the temperature dependence of D and K. The activation energy for diffusion (0.7 eV with an error range from 0.58 to 0.98 eV) was very close to the activation energy for interface migration (0.6 eV with an error range from 0.55 to 0.67 eV). Probably, the prevailing diffusion mechanism at these temperatures is short circuit diffusion.
4. The diffusion constants $D^- = 5.5 \times 10^{-13}$ cm^2/s and the activation energy (0.7 eV) are consistent with previous studies of diffusion in dislocation-rich α_2.
5. The interface mobility can be calculated from K. The interface accommodation factor estimated from the temperature dependence of K is $\sim 10^{-14}$.

ACKNOWLEDGMENTS

This research was supported financially by NASA through Grant No. NAG 9-45. The authors would like to thank Dr. J. R. Michael of Homer Research Laboratoy, Bethlehem Steel Corporation (now at Sandia National Laboratories), and Dr. C. E. Lyman of Lehigh University for the assistance with the VG.

REFERENCES

1. A.D. Romig, Jr. and J.I. Goldstein: *Metall. Trans. A*, 1980, vol. 11A, pp. 1151-59.
2. J.I. Goldstein and R.E. Ogilvie: *Trans. TMS-AIME*, 1965, vol. 233, pp. 2083-87.
3. L. Kaufman and M. Cohen: *Trans. AIME*, 1956, vol. 206, pp. 1393-401.
4. H.I. Aaronson: *Decomposition of Austenite by Diffusional Process*, Interscience, New York, NY, 1962, p. 387.
5. J.W. Martin and R.D. Doherty: *Stability of Microstructure in Metallic Systems*, Cambridge University Press, Cambridge, United Kingdom, 1976, pp. 18-50.
6. D.A. Porter and K.E. Easterling: *Phase Transformation in Metals and Alloys*, Van Nostrand Reinhold, Wokingham, Berkshire, United Kingdom, 1981, pp. 177-90.
7. J. Zhang, D.B. Williams, and J.I. Goldstein: *Metall. Mater. Trans. A*, 1994, vol. 25A, pp. 1627-37.
8. J. Noye: *Numerical Solutions to Partial Differential Equations*, North-Holland Publishing, Amsterdam, 1975.
9. W.D. Murray and F. Landis: *Trans. ASME, J. Heat Transfer*, 1959, vol. 81, pp. 106-12.
10. C. Narayan and J.I. Goldstein: *Metall. Trans. A*, 1984, vol. 15A, pp. 861-65.
11. A.D. Romig, Jr. and J.I. Goldstein: *Metall. Trans. A*, 1981, vol. 12A, pp. 243-51.
12. J.I. Goldstein, D.E. Newbury, P. Echlin, D.C. Joy, A.D. Romig Jr., C.E. Lyman, C. Fiori, and E. Lifshin: *Scanning Electron Microscopy and X-ray Microanalysis*, 2nd ed., Plenum Press, New York, NY, 1992.
13. J.R. Michael: *Microbeam Analysis—1988*, San Francisco Press Inc., San Francisco, CA, 1988, pp. 60-64.
14. J.I. Goldstein, C.E. Lyman, and J. Zhang: *Microbeam Analysis—1990*, San Francisco Press Inc., San Francisco, CA, 1990, pp. 265-73.
15. G. Cliff and G.W. Lorimer: *J. Microsc.*, 1975, vol. 103, pp. 203-07.
16. J. Zhang: Ph.D. Dissertation, Lehigh University, Bethlehem, PA, 1991.
17. S.J.B. Reed: *Ultramicroscopy*, 1982, vol. 7, pp. 405-09.
18. J.R. Michael, D.B. Williams, C.F. Klein, and R. Ayer: *J. Microsc.*, 1990, vol. 160, pp. 41-53.
19. V. Saikumar and J.I. Goldstein: *Geochim. Cosmochim. Acta*, 1988, vol. 52, pp. 715-26.
20. D.C. Dean and J.I. Goldstein: *Metall. Trans. A*, 1986, vol. 17A, pp. 1131-38.
21. G.C. Weatherly: *Acta Metall.*, 1971, vol. 19, pp. 181-92.
22. H.I. Aaronson, C. Laird, and K.R. Kinsman: *Phase Transformations*, ASM, Metals Park, OH, 1970, pp. 313-36.